Optics Letters

Surface lattice resonances in second-harmonic generation from metasurfaces

Robert Czaplicki,[1,*] Antti Kiviniemi,[1] Janne Laukkanen,[2] Joonas Lehtolahti,[2] Markku Kuittinen,[2] and Martti Kauranen[1,3]

[1]Department of Physics, Tampere University of Technology, P.O. Box 692, FI-33101 Tampere, Finland
[2]Institute of Photonics, University of Eastern Finland, P.O. Box 111, FI-80101 Joensuu, Finland
[3]e-mail: martti.kauranen@tut.fi
*Corresponding author: robert.czaplicki@tut.fi

Received 23 February 2016; accepted 9 May 2016; posted 16 May 2016 (Doc. ID 259863); published 2 June 2016

We investigate the role of surface-lattice resonances (SLRs) in second-harmonic generation (SHG) from arrays of metal nanoparticles. The SLRs affect the generated signal when the sample is rotated away from normal incidence. The adjustment of the incident angle tunes the SLRs to the fundamental wavelength for SHG and improves the quality of the resonance for better resonance enhancement of SHG. Compared to normal incidence, an enhancement by a factor of 10 is observed. However, at certain incident angles, the enhancement is interrupted by diffraction anomalies, which redirect light into the substrate, increasing radiation damping and compromising the quality of the resonance.

OCIS codes: (160.3918) Metamaterials; (190.4160) Multiharmonic generation; (240.6680) Surface plasmons; (260.5740) Resonance.

http://dx.doi.org/10.1364/OL.41.002684

The oscillations of conduction electrons, known as plasmons, determine the optical properties of metal nanostructures. For nanoparticles, the oscillations are confined, giving rise to localized surface-plasmon resonances (LSPRs). Such resonances depend on the size, shape, and environment of the particles. When the nanoparticles are arranged in arrays, as is usually the case for metasurfaces, the LSPRs are modified by the presence of adjacent particles. In addition, when the period of the array is near the LSPR wavelength of the particle, surface-lattice resonances (SLRs) may occur [1–5]. This can give rise to very sharp spectral features, which are linked to the appearance or disappearance of diffraction orders in the optical response. The features arise from coupling between LSPRs of the particles and diffraction anomalies [1,4]; therefore, they are very sensitive to the angle of incidence into the structure [1,3,6,7].

The resonances give rise to strong local electromagnetic fields near the particles (hot spots), which can be beneficial for nonlinear optical effects, including second-harmonic generation (SHG). As an even-order nonlinear process, SHG is forbidden in centrosymmetric materials. This symmetry rule, however, makes SHG useful to study surfaces and thin films, but the surface nonlinearity can typically be accessed only at oblique angle of incidence. To break the centrosymmetry of metasurfaces, the nanoparticles (meta-atoms) are usually designed to appear noncentrosymmetric even when probed at normal incidence, allowing experiments without coupling to the traditional surface nonlinearity. For such meta-atoms of low symmetry, their arrangement in the array may influence the symmetry and dimensions of the unit cell, which may lead to lattice effects and change the SHG response [8,9].

The presence of resonances is crucial to boost the nonlinearity of metasurfaces [10,11], with the possible exception of specific particle geometries and nonlinear signals [12,13]. The quality of the resonance (height, width) as well as the detuning of the fundamental wavelength from the line center therefore play a vital role in the achievable resonance enhancement of nonlinear processes [11,14]. High-quality narrow resonances can be achieved, e.g., by improving the fabrication process [15], and further narrowing can be realized by varying the lattice constant or by changing the angle of incidence of the light beam into the structure [1,3,6,7]. Very few nonlinear studies with varying incident angles, however, have been performed on metasurfaces. For SHG, such studies have been limited to nanoapertures [16,17], split-ring resonators [18], and G-shaped nanostructures [19]. Theoretical analysis of angle-dependent SHG from nanoparticles has also been presented [20]. However, the role of SLRs to the nonlinear responses has not yet been fully explored.

In this Letter, we show that the SLRs of the structure can significantly modify the SHG response. For our particular structures, the SLR can be sharpened and tuned to our laser wavelength by increasing the angle of incidence, thereby improving the resonance enhancement. However, the angular dependence is also modified by the occurrence of diffraction anomalies at the fundamental or second-harmonic wavelength. In general, these anomalies ultimately compromise the efficiency of the SHG signal at large angles of incidence when a propagating diffraction order opens for the fundamental wavelength. Nevertheless, the optimum angle of incidence can enhance the SHG efficiency by a factor of 10 compared to normal incidence.

Our sample is a 1 mm × 1 mm metasurface fabricated by electron-beam lithography and lift off, and consists of an array of L-shaped gold nanoparticles. The particles are equally distributed in both planar directions (x and y) of the 2D array with a period of 500 nm (Fig. 1). The particles are 20 nm thick and have equally long (275 nm) and wide (100 nm) arms. The length of the arms determines the spectral position of the resonances along the symmetry axis (y) and orthogonal to it (x).

The measurements of the linear response (transmitted light in $-z$ direction; sample illuminated from the nanoparticle side) revealed the positions of the plasmon resonances, which also determine the resonance condition for the SHG response. The shorter wavelength resonance (y) at 990 nm is due to oscillation along the arms of the L-shape. Therefore the resonant SHG tensor component (yyy; where the first letter describes the polarization of second-harmonic light and the second and third letters define the polarization of fundamental light) is detected when both the incident and SH light are y-polarized [9]. Other tensor components possible for our sample are yxx, xxy, and xyx (allowed by symmetry) and xxx, xyy, xxy, and xyx (forbidden by symmetry). Here, we will focus on the resonant and symmetry-allowed yyy component.

We studied the linear response of our sample for different incident angles and using the two configurations ($\phi = 0°$ and $\phi = -90°$) shown in Fig. 2, where the incident angle is varied by rotating the sample about the y- or x-axis, respectively. The results corresponding to the configuration in Fig. 2(a) are presented in Fig. 3. The spectra related to the configuration in Fig. 2(b) are qualitatively similar (not shown here).

When the incident angle is increased, the following can be observed (Fig. 3): (i) at normal incidence [Fig. 3(a)], the diffraction anomalies are considerably blueshifted compared to the LSPR, which does not allow the excitation of the SLRs [21]; (ii) when the incident angle is increased, the diffraction anomaly redshifts approaching the LSPR [Figs. 3(c) and 3(d)]. This improves the excitation of the particles in the array and reduces the energy required for excitation; (iii) due to the reduction in energy, the resonance redshifts, as observed

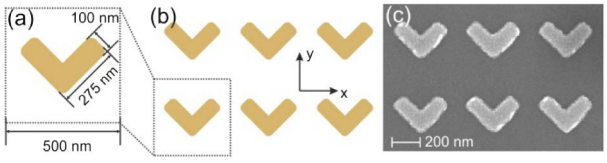

Fig. 1. (a) Dimensions, (b) array design, and (c) scanning electron microscopy image of the studied sample. The scale bar and coordinate system are also shown.

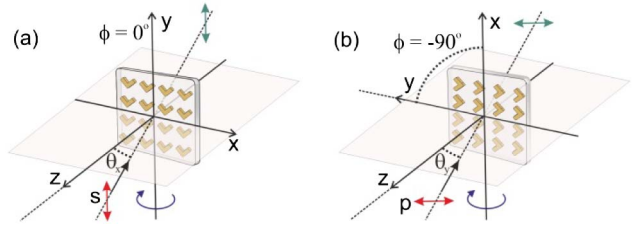

Fig. 2. Experimental geometry for two configurations: (a) $\phi = 0°$ and (b) $\phi = -90°$.

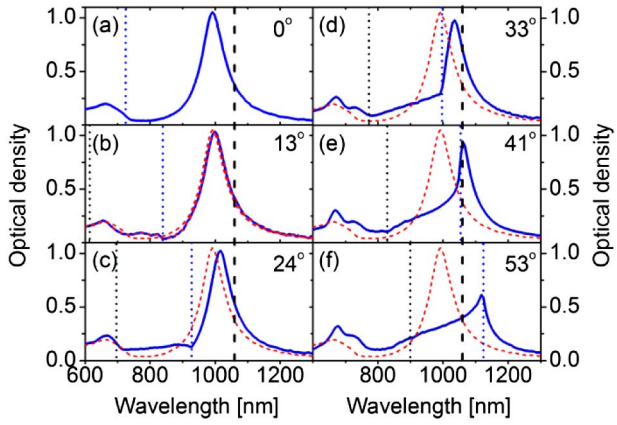

Fig. 3. y-polarized extinction spectra measured at (a) 0°, (b) 13°, (c) 24°, (d) 33°, (e) 41°, and (f) 53° incident angles. The vertical black dashed line indicates the position of the fundamental wavelength for SHG (1060 nm) and the vertical dotted lines indicate the spectral positions of diffraction anomalies [for first order of diffraction (−1, 0) into the substrate (blue) and air (black)]. The reference extinction spectrum measured at normal incidence (red dashed line) is shown in each panel.

previously [22]; (iv) the intensity of the resonance decreases [23]; (v) the resonance becomes narrower and the symmetry is affected by change in curvature at its left side leading to Fano-type shape of the resonance (Fig. 3) [2,24]. The change in the shape is due to the appearance of the first order of diffraction, which leads to an increase in the radiated power from the array [25] through Rayleigh–Wood anomalies [26]; (vi) SLRs can be observed when the position of the diffraction anomaly is close to the position of the LSPR.

The redshift of the resonance tunes its spectral position toward the fundamental wavelength of 1060 nm, matching the fundamental wavelength at 41° [Fig. 3(e)]. At the same time, the position of the diffraction anomaly is also redshifted, allowing for the formation of a SLR [22], which in turn leads to significant narrowing of the resonance.

Since our sample is a square array, it can be treated as a two-dimensional grating, for which the positions of the diffraction anomalies can be calculated by applying the Bragg condition. For the direction of incident light in the x–z plane, the condition for diffraction anomalies is [22]

$$\lambda_{(i,0)} = G\left(\frac{n}{|i|} - \frac{\sin\theta_x}{i}\right), \tag{1}$$

where G is the period of the array ($G_x = G_y = G$), θ_x is the angle of incidence, n is the refractive index of the medium of propagation [the refractive index of the incident medium (air) is assumed to be $n_{\text{inc}} = 1$], and i is an integer related to the diffraction order (note that subscript 0 indicates the diffraction order in the y direction; $j = 0$). When the incident wavelength matches the $\lambda_{(i,0)}$, the diffraction orders propagate along the sample plane either in air (reflected orders) or in the substrate (transmitted orders) [1], as depicted in Fig. 4.

Figure 5 shows the wavelengths for the opening of diffraction orders for air and substrate calculated using Eq. (1). The period of our sample is $G = 500$ nm and the refractive index of the glass substrate $n = 1.45$ (note, however, that the refractive index exhibits some wavelength dependence, which is

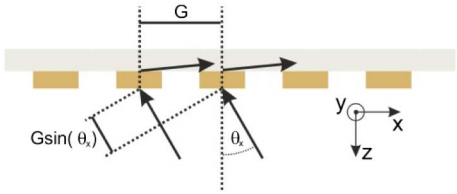

Fig. 4. Sketch of the sample geometry with the incident field at oblique angle θ_x.

unimportant for the main conclusions). For the incident wavelength of $\lambda = 1060$ nm, the particular angles where the anomalies occur are $\theta_x = 42°$ [grating order: $(-1, 0)$] and in the air, the angle becomes $\theta_x = 4°$ ($n = 1$). However, for the SH light of $\lambda = 530$ nm the anomaly occurs at $\theta_x = 23°$ [grating order: (1,0)], see Fig. 5.

In order to study the influence of the SLRs on the SHG response, we used the configurations presented in Fig. 2. The light before and after the sample was linearly polarized (s, $\phi = 0°$ or p, $\phi = -90°$) to interact with the component yyy of the tensor describing SHG, which is allowed by the symmetry group of the sample and resonant with the fundamental wavelength. During the measurements the angle of incidence (θ_x or θ_y) was changed when the sample was rotated about the y- ($\phi = 0°$) or x-axis ($\phi = -90°$), respectively.

The SHG response depends strongly on the incident angle growing up to 41°–42°, where it reaches a maximum after which it dwindles quickly to a much lower value [Fig. 6(a)]. In addition to the maximum at 41°, a weak anomalous feature is observed at 24° [Fig. 6(a)]. Irregular features are also observed at similar angles (22° and 41°) in the s-polarized fundamental light transmitted through the sample. At 22° the transmission drops abruptly and decreases further reaching a minimum at 41° [Fig. 6(b)].

Analogous results were obtained for the azimuthally rotated [by 90°, Fig. 2(b)] sample (Fig. 7). The maximum at 41° is now even more pronounced for the positive angles (note that a positive angle corresponds to the corner of the L-shape toward $+z$ direction while the arms are toward $-z$ direction). Also, the feature at 24° is noticeable here (Fig. 7). Furthermore,

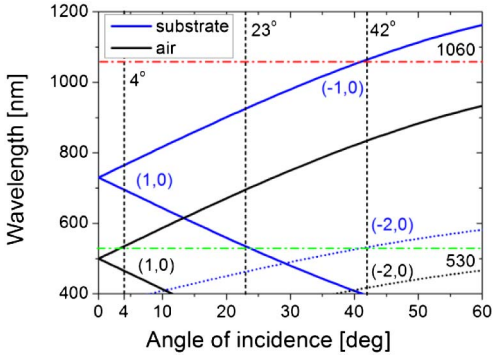

Fig. 5. Angular dependence of diffraction anomalies calculated with Eq. (1) for grating orders in the substrate (blue) and in air (black). The horizontal dashed-dotted lines show the fundamental and SH wavelengths, respectively, and the vertical dashed lines show the most interesting incident angles. The numbers in the parentheses indicate diffraction orders [(i, j), $j = 0$].

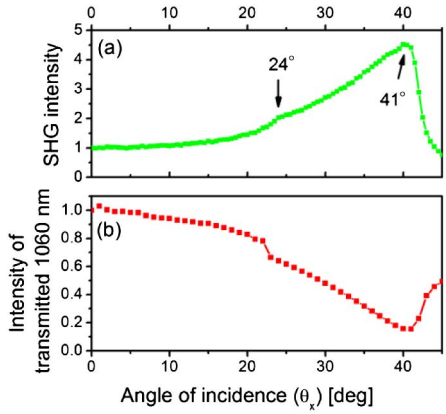

Fig. 6. (a) SHG signal and (b) intensity of s-polarized laser light (1060 nm) transmitted through the sample as functions of angle of incidence θ_x (normalized to response at 0°).

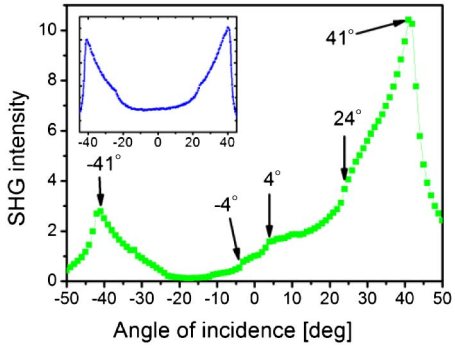

Fig. 7. SHG intensity as function of incident angle normalized to the response at normal incidence for the azimuthal orientation $\phi = -90°$. The SHG signal and incident light were p-polarized (yyy at normal incidence). The noise level is smaller than the data points. Inset shows the full angle dependence of the SHG signal from Fig. 6(a).

the signal grows irregularly revealing small anomalies at ±4°, corresponding to a diffraction order in air. The results for this configuration are highly asymmetric leading to stronger signals for positive angles θ_y. An enhancement by a factor of 10 is observed in this case, while the enhancement is about 3 for the negative angles. Due to the strong asymmetry of the signal for this $\phi = -90°$ configuration, we reconfirmed that the results for the $\phi = 0°$ configuration are symmetric (inset in Fig. 7). The small deviation (10%) in the SHG between negative and positive incident angles is due to difficulties in the precise alignment of the experiment.

The strong enhancement for the positive angles can be explained by the SHG radiation pattern of L-shaped particles. In the case of y-polarized input, the radiation is oriented toward $+y \pm z$ directions [27,28]. Thus, by increasing the angle of incidence toward positive angles [Fig. 7], the direction of detection is approaching the direction of maximum SHG radiation from individual particles. At the same time, the SHG wavelets from individual particles are phase-matched in the same direction [29].

It is important to note that oblique incident angles allow SHG also from structures that appear centrosymmetric at

normal incidence. In some cases, the SHG efficiency can be even higher than from noncentrosymmetric particles [20]. However, for the polarization configuration of Fig. 2(a), the *yyy* signal from centrosymmetric particles remains forbidden for any incident angle. In addition, our control measurements performed on arrays of off-resonant centrosymmetric nanobars showed negligible SHG for the whole angular range.

The results show that with the increasing incident angle, the SHG signal from arrays of L-shaped particles grows as the resonance is tuned toward the fundamental wavelength. At the same time the quality of the resonance improves due to the SLRs. The increase of SHG, however, is disturbed by the appearance of diffraction anomalies at particular incident angles (23° and 42°). At 23° the (1,0) substrate diffraction order for SH light appears and the rate of increase of the SHG signal is slowed down after 24°. Passing through the 24° angle, the SHG still rises up until 41°–42°, where the $(-1, 0)$ substrate diffraction order for fundamental wavelength appears and the diffracted waves travel along the surface of the substrate. The increase in the SHG signal is thus interrupted by the diffraction anomalies, which eventually give rise to an abrupt drop in the signal. This general behavior is further modified depending on whether the sample is rotated about the symmetry axis (y) or the orthogonal axis (x). In the latter case, the asymmetry of the SHG radiation pattern favors the emission for positive but not negative incident angles.

In conclusion, we have used second-harmonic generation to study the role of SLRs in the second-order nonlinear optical response of metasurfaces. The second-harmonic signal can be enhanced by the SLRs when the sample is rotated away from normal incidence. This occurs when the SLR gives rise to a narrow resonance matching the wavelength of the fundamental laser beam. SHG enhancement by a factor of 10 is obtained at the optimum angle of incidence compared to normal incidence when the signal is detected in the direction of SHG radiation. The enhancement is, however, interrupted by diffraction anomalies, which are responsible for redirection of light into the substrate. This causes radiative damping and loss of the quality of the resonance for incident angles exceeding the SLR conditions. More studies are needed to fully understand how SLRs can be improved for optimum enhancement of nonlinear responses.

Funding. Academy of Finland (265682, 287651).

Acknowledgment. This work was performed in the context of the European COST Action MP1302 Nanospectroscopy.

REFERENCES

1. V. G. Kravets, F. Schedin, and A. N. Grigorenko, Phys. Rev. Lett. **101**, 087403 (2008).
2. B. Auguié and W. L. Barnes, Phys. Rev. Lett. **101**, 143902 (2008).
3. Y. Chu, E. Schonbrun, T. Yang, and K. B. Crozier, Appl. Phys. Lett. **93**, 181108 (2008).
4. F. J. García de Abajo, Rev. Mod. Phys. **79**, 1267 (2007).
5. A. D. Humphrey and W. L. Barnes, Phys. Rev. B **90**, 075404 (2014).
6. S. Linden, J. Kuhl, and H. Giessen, Phys. Rev. Lett. **86**, 4688 (2001).
7. W. Zhou and T. W. Odom, Nat. Nanotechnol. **6**, 423 (2011).
8. H. Husu, R. Siikanen, J. Mäkitalo, J. Lehtolahti, J. Laukkanen, M. Kuittinen, and M. Kauranen, Nano Lett. **12**, 673 (2012).
9. R. Czaplicki, H. Husu, R. Siikanen, J. Mäkitalo, J. Laukkanen, J. Lehtolahti, M. Kuittinen, and M. Kauranen, Phys. Rev. Lett. **110**, 093902 (2013).
10. F. B. P. Niesler, N. Feth, S. Linden, and M. Wegener, Opt. Lett. **36**, 1533 (2011).
11. M. Kauranen and A. V. Zayats, Nat. Photonics **6**, 737 (2012).
12. J. Berthelot, G. Bachelier, M. Song, P. Rai, G. Colas des Francs, A. Dereux, and A. Bouhelier, Opt. Express **20**, 10498 (2012).
13. R. Czaplicki, J. Mäkitalo, R. Siikanen, H. Husu, J. Lehtolahti, M. Kuittinen, and M. Kauranen, Nano Lett. **15**, 530 (2015).
14. B. Metzger, M. Hentschel, M. Lippitz, and H. Giessen, Opt. Lett. **37**, 4741 (2012).
15. R. Czaplicki, M. Zdanowicz, K. Koskinen, J. Laukkanen, M. Kuittinen, and M. Kauranen, Opt. Express **19**, 26866 (2011).
16. M. Airola, Y. Liu, and S. Blair, J. Opt. A **7**, S118 (2005).
17. S. G. Rodrigo, V. Laliena, and L. Martín-Moreno, J. Opt. Soc. Am. B **32**, 15 (2015).
18. M. W. Klein, M. Wegener, N. Feth, and S. Linden, Opt. Express **15**, 5238 (2007) [Erratum: Opt. Express **16**, 8055 (2008)].
19. E. A. Mamonov, I. A. Kolmychek, S. Vandendriessche, M. Hojeij, Y. Ekinci, V. K. Valev, T. Verbiest, and T. V. Murzina, Phys. Rev. B **89**, 121113 (2014).
20. C. Cirací, E. Poutrina, M. Scalora, and D. R. Smith, Phys. Rev. B **86**, 115451 (2012).
21. T. V. Teperik and A. Degiron, Phys. Rev. B **86**, 245425 (2012).
22. T. W. W. Mass and T. Taubner, ACS Photonics **2**, 1498 (2015).
23. V. Liberman, R. Adato, A. Mertiri, A. A. Yanik, K. Chen, T. H. Jeys, S. Erramilli, and H. Altug, Opt. Express **19**, 11202 (2011).
24. M. Kataja, T. K. Hakala, A. Julku, M. J. Huttunen, S. van Dijken, and P. Torma, Nat. Commun. **6**, 7072 (2015).
25. R. Adato, A. A. Yanik, C.-H. Wu, G. Shvets, and H. Altug, Opt. Express **18**, 4526 (2010).
26. L. Rayleigh, Philos. Mag. Ser. 6 **14**(79), 60 (1907).
27. J. Mäkitalo, S. Suuriniemi, and M. Kauranen, Opt. Express **19**, 23386 (2011).
28. C. Forestiere, A. Capretti, and G. Miano, J. Opt. Soc. Am. B **30**, 2355 (2013).
29. D. de Ceglia, M. A. Vincenti, C. De Angelis, A. Locatelli, J. W. Haus, and M. Scalora, Opt. Express **23**, 1715 (2015).